

Article

A Systematic Study of Estimating Potato N Concentrations Using UAV-Based Hyper- and Multi-Spectral Imagery

Jing Zhou ¹, Biwen Wang ¹, Jiahao Fan ¹, Yuchi Ma ¹, Yi Wang ² and Zhou Zhang ^{1,*}¹ Biological Systems Engineering, University of Wisconsin-Madison, Madison, WI 53706, USA² Department of Horticulture, University of Wisconsin-Madison, Madison, WI 53706, USA

* Correspondence: zzhang347@wisc.edu

Abstract: Potato growth depends largely on nitrogen (N) availability in the soil. However, the shallow-root crop coupled with its common cultivation in coarse-textured soils leads to its poor N use efficiency. Fast and accurate estimations of potato tissue N concentrations are urgently needed to assist the decision making in precision fertilization management. Remote sensing has been utilized to evaluate the potato N status by correlating spectral information with lab tests on leaf N concentrations. In this study, a systematic comparison was conducted to quantitatively evaluate the performance of hyperspectral and multispectral images in estimating the potato N status, providing a reference for the trade-off between sensor costs and performance. In the experiment, two potato varieties were planted under four fertilization rates with replicates. UAV images were acquired multiple times during the season with a narrow-band hyperspectral imager. Multispectral reflectance was simulated by merging the relevant narrow bands into broad bands to mimic commonly used multispectral cameras. The whole leaf total N concentration and petiole nitrate-N concentration were obtained from 160 potato leaf samples. A partial least square regression model was developed to estimate the two N status indicators using different groups of image features. The best estimation accuracies were given by reflectance of the full spectra with 2.2 nm narrow, with the coefficient of determination (R^2) being 0.78 and root mean square error (RMSE) being 0.41 for the whole leaf total N concentration; while, for the petiole nitrate-N concentration, the 10 nm bands had the best performance ($R^2 = 0.87$ and RMSE = 0.13). Generally, the model performance decreased with an increase of the spectral bandwidth. The hyperspectral full spectra largely outperformed all three multispectral cameras, but there was no significant difference among the three brands of multispectral cameras. The results also showed that spectral bands in the visible regions (400–700 nm) were the most highly correlated with potato N concentrations.

Keywords: potato; hyperspectral; multispectral; nitrogen; remote sensing; spectral synthesis

Citation: Zhou, J.; Wang, B.; Fan, J.; Ma, Y.; Wang, Y.; Zhang, Z. A Systematic Study of Estimating Potato N Concentrations Using UAV-Based Hyper- and Multi-Spectral Imagery. *Agronomy* **2022**, *12*, 2533. <https://doi.org/10.3390/agronomy12102533>

Academic Editor: Salvatore Filippo Di Gennaro

Received: 22 September 2022

Accepted: 14 October 2022

Published: 17 October 2022

Publisher's Note: MDPI stays neutral with regard to jurisdictional claims in published maps and institutional affiliations.



Copyright: © 2022 by the authors. Licensee MDPI, Basel, Switzerland. This article is an open access article distributed under the terms and conditions of the Creative Commons Attribution (CC BY) license (<https://creativecommons.org/licenses/by/4.0/>).

1. Introduction

There has been unwitnessed pressure on agriculture and natural resources due to the anticipated world population (9.8 billion by 2050) and adverse agricultural environments [1,2]. Though with improved production in major crops yearly, it still remains challenging to provide sufficient nutritious food without generating negative environmental impacts [3]. Potatoes (*Solanum tuberosum* L.) are an essential and commonly non-grain food in the world and contain high food energy and complex carbohydrates [4]. Over 359 million metric tons of potatoes were produced worldwide in 2020. In the United States, around 23 million metric tons of potatoes were harvested from about 370 thousand hectares, yielding around USD 4 billion in cash values [5].

Potato growth depends largely on its nitrogen (N) availability, as N is involved in the process of photosynthesis and the production of proteins and nucleic acids. However, the shallow-root system coupled with their common cultivation in coarse-textured soils leads to poor N use efficiency in potato plants [6]. N deficiency during potato growth

causes premature leaf senescence, decreased tuber yield, and lower starch contents [7]. Additionally, without enough N uptake, plants are more susceptible to biotic and abiotic stresses. On the other side, an excessive application of N would cause poor skin set, lead to over-lush vegetation growth and delay tuber maturation, and thus reduce tuber yield. Moreover, oversupplied N might leach into groundwater in the form of nitrate with heavy rainfall or irrigation activities. Long-term exposure to nitrate-contaminated water brings health risks to humans and animals [8]. Therefore, precise and timely decisions on N fertilization are crucial in potato production to maximize the tuber yield and quality and minimize N pollution [6].

Decision making for N fertilization includes considerations on the rate and timing of N applications coupled with irrigation management [9], which requires season-long and timely monitoring of the plant N status. Petiole nitrate-N concentration has been commonly used to guide N applications by potato growers in the Midwest. Petioles are the tissues that attach the leaf blades to the stems, and N is transported in the form of nitrate within petioles [10]. The petiole nitrate-N concentration reflects whether potato crops are absorbing enough nutrients [11]. However, the measurements are highly variable, depending on the sampling conditions (e.g., timing, weather, soil, and potato growth stages), and solely relying on it might suppress tuber bulking but lead to excessive vine growth [12,13]. In contrast to petiole, leaf stores N cumulatively as proteins and amino acids [14]. Thus, the whole leaf total N concentration can be used as a complementary indicator to monitor whether potato plants have taken sufficient nutrients accumulatively [10,12].

Remote sensing has been utilized to evaluate crop N status as an alternative to the ground analysis of plant tissues. Handheld spectrometers are one of the widely used remote sensors due to their high spectral resolution and easy accessibility. Potato N concentrations were shown to be linearly correlated with particular regions and combinations of spectral reflectance values from the handheld spectrometers. Yang et al. [15] found that potato canopy N concentrations are mainly sensitive to the ultraviolet region (340–400 nm) and visible region (450–690 nm). Clevers and Kooistra [16] calculated a group of vegetation indices (VIs) with narrow spectral bands and those combined with near-infrared (NIR) (750–800 nm) and red-edge regions (690–730 nm) could explain over 70% of the variations in the potato N concentrations. The best linear estimators were the ratios of NIR to red-edge ($CI_{red-edge}$), and they performed similarly regardless of the central bands and bandwidth (3, 30, and 50 nm) taken from the two regions. A similar conclusion was made by Morier et al. [17] that the red-edge spectral region was sensitive to potato N concentrations, and it was highly related to the total tuber yield. Moreover, Herrmann et al. [18] found the 1510 nm band in the shortwave infrared region (1200–2500 nm) is the most relevant one. The combined reflectance from the 1510 and 660 nm bands significantly correlated with the potato N concentrations (coefficient of determination $R^2 = 0.72$ – 0.75). Similarly, significant linear relationships between the spectrometer-derived VIs and ground measured potato N concentrations were also reported by Sun et al. [19] and Zhou et al. [20].

Hyperspectral cameras are another popular tool and have been extensively adopted in the field of precision agriculture. They help to save a significant amount of effort in field data collection by taking image frames rather than single points and leveraging the flexibility in cooperating with imaging platforms, such as unmanned aerial vehicles (UAVs) or ground mobile facilities, largely expanding the spatial and temporal resolutions for in-field crop monitoring. Cohen et al. [21] obtained an excellent agreement between the ground measured and estimated the leaf N concentration and petiole nitrate-N concentration (R^2 being 0.86 and 0.74, respectively). The estimates were from a partial least squares regression (PLSR) model taking 210 aerial hyperspectral narrow-band images as predictors. Similarly, an R^2 of 0.79 was reported for estimating the potato leaf N concentration by using PLSR and 63 hyperspectral bands. It was also found that the canopy-scale imagery outperformed the single-point spectral data in the experiments [22].

Multispectral cameras have been considered an alternative to hyperspectral cameras. Nigon et al. [6] reported that the multispectral-derived VIs collected using manned aerial

vehicles at 235 m can account for 40–80% of the variations of potato leaf N concentrations. In comparison, the multispectral imagery in [23] was not able to differentiate plots with different N fertilization rates that were detectable by a chlorophyll meter. Compared to the hyperspectral cameras, the multispectral cameras have discrete and broad spectral bands, and consequently, they are not able to capture spectral information as detailed as the hyperspectral cameras [24,25]. However, data from multispectral cameras are more available due to their low costs in manufacturing, image processing, data management, and storage. Additionally, multispectral cameras are more portable and flexible to be mounted on a variety of imaging platforms.

The performances of multispectral and hyperspectral imagery have been compared in previous studies in terms of estimating crop traits. The hyperspectral data were found to perform better than the multispectral data in estimating leaf area index [26], crop mapping [27], crop biomass [28], and leaf N concentration [25]. Whereas, in other cases on the estimation of vegetation properties, data from both platforms performed similarly [24,29,30]. However, it is not a fair comparison of the performance simply by regressing the sensory data from two or more cameras to the same set of ground measurements. Data collected from different sensors could be affected by factors such as plant physiological changes and environmental variations [30]. Even if the data are collected at the same time, potential influences could be derived from the mechanical factors, such as radiometric resolution and exposure settings, as well as the image processing procedures, including geometric and radiometric corrections and mosaic.

This study hypothesizes that narrow and contiguous spectral bands in the visible to NIR ranges could perform better in estimating potato N concentrations than the broad and discrete bands in the same range. Thus, to provide a reference for the trade-off between sensor costs and performance, we simulated a group of spectral reflectance values of multispectral bands using the hyperspectral reflectance to quantitatively compare their accuracies in estimating laboratory measured leaf total N concentration and petiole nitrate-N concentrations of potato samples. The objectives of this paper include: (1) evaluate the potato N variability under different fertilization treatments over time, (2) compare the performances of narrow and broad hyperspectral bands, (3) compare the performances of narrow hyperspectral bands and simulated multispectral bands, and (4) identify the spectral regions effective in estimating potato N concentrations.

2. Methods and Materials

2.1. Field Experiments

The field experiment was conducted in 2021 at the Hancock Agricultural Research Station (HARS), Hancock, WI, USA. The experiment site is characterized by sandy and coarse soil texture with a relatively shallow water table and a low organic matter content [10,31]. During the growing season from May to September, the average temperature was 18.9 °C and total precipitation was 566 mm [Data retrieved from <https://enviroweather.msu.edu/weather.php?stn=hck>, (accessed on 11 February 2022)].

The experiment was conducted in a split-plot design, as shown in Figure 1. The field has one non-fertilization strip and one fertilization strip. Within each strip, two N rates, as shown in Table 1, were randomized to the whole plot with four replicates. The non-fertilization treatments were done by side-dressing the dry fertilizer on both sides of the hills, except for the starter and hilling. For the fertilization treatments, liquid N (32% urea ammonium nitrate) was applied through irrigation water four times during the early and mid-tuber bulking stages. Two cultivars, Snowden (chipping potato cultivar) and Colomba (yellow potato cultivar), were randomized to each subplot.

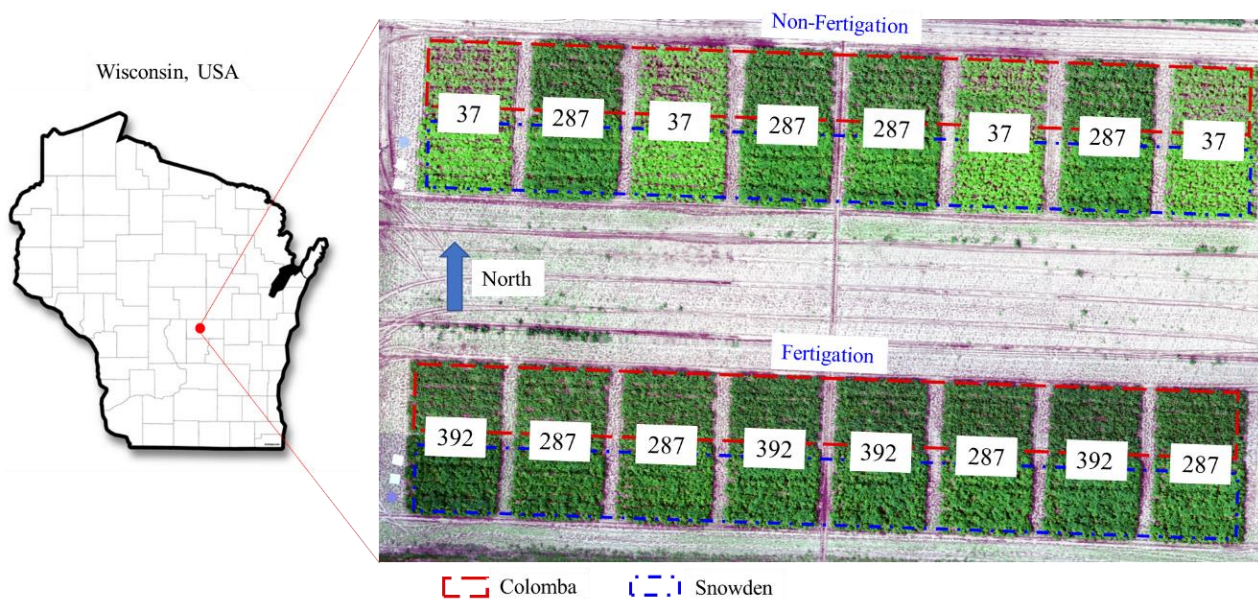


Figure 1. Experimental site and design.

Table 1. Nitrogen treatments and schedule.

Fertigation	Seasonal Total N Rate	Planting	Emergence (Hilling)	Tuber Initiation	Fertigation Date			
		23 April	12 May	2 June	30 June	10 July	20 July	30 July
No	37	37	-	-	-	-	-	-
No	287	37	85	165	-	-	-	-
Yes	287	37	85	30	34	34	34	34
Yes	392	37	85	134	34	34	34	34

Unit: kg/ha.

The dimensions of the whole field were 41 × 78 m. Each subplot has eight rows, with each row being 7.6 m long and 0.9 m wide. Seed spacing was 23 cm for Colomba and 30 cm for Snowden. Starting from the outside alley, the third and fourth rows were selected for sampling the petiole and whole leaf. Seed tubers were planted on 23 April and harvested on 15 September 2021. Besides N management, all other production practices, including irrigation and pest control, were based on UW Extension recommendations.

2.2. Image Acquisition and Ground Sampling

Hyperspectral images were collected under clear sky conditions five times in the growing season on 06/30, 07/20, 07/29, 08/03, and 08/12, approximately 69, 89, 98, 103, and 112 days after planting (DAP), respectively. The images were taken by a Headwall Nano-Hyperspec push broom hyperspectral camera, which has 274 spectral bands from 400 to 1000 nm. A Global Navigation Satellite System (GNSS)-aided Inertial Navigation System was used to provide the position and orientation for data georeferencing. All the devices were carried on a DJI Matrice 600 Pro hexacopter. The UAV flew at 60 m above the ground level with a forward speed of 6 m/s. The flight plan was predefined in a flight control App Field Agent. Before each image collection, three calibration panels with 11%, 32%, and 56% reflectivity were placed in the field for radiometric correction.

Ground data sampling was conducted between 8 am and 12 pm on the same day that UAV images were collected. Potato petioles and whole leaf samples were collected before N fertigation if there was fertigation scheduled on those days (Table 1). In each sampling time, 20 plants were randomly selected from individual subplots for measuring the petiole

nitrate-N concentration. Petioles of the fourth healthy leaf from the shoot top were picked for each plant. Similarly, another 20 plants per subplot were randomly selected for the whole N concentration, and the fourth healthy leaf from the shoot top was taken as the whole leaf sample. All plant tissues were dried at 70 °C for at least 24 h. The dried petioles and whole leaves were then ground separately. The petioles nitrate-N analysis (% dry weight basis) was performed using the method published by the University of Wisconsin Soil and Forage Lab [32]. The total N in the whole leaves (% dry weight basis) was analyzed using an Elemental Combustion System.

2.3. Image Processing

The hyperspectral images were corrected geometrically and radiometrically using processing software (SpectraView II 1.1.39) provided by the sensor manufacturer. The images were first orthorectified and mosaiced in SpectralView using the georeferencing data collected simultaneously with the image. In SpectralView, the raw image pixel numbers were converted to radiance and then to reflectance in an automatic process after visually identifying the calibration panels from the raw image. Based on the visual examination, image pixels with reflectance values lower than 15% at the 800 nm wavelength were considered as background (e.g., shadow and soil), and they were removed for each of the five image collections. Individual potato plots were segmented from the corrected hyperspectral mosaic for each image collection by manually drawing a rectangular cropping area around the plot boundaries, leading to a total of 160 individual plots. The average reflectance values of each plot were then calculated for all the 274 wavelengths.

2.4. Synthetization of Multispectral Image Features

The hyperspectral reflectance values were used to synthesize the reflectance for three popular multispectral cameras, namely the embedded camera on P4 Multispectral (DJI, Shenzhen, Guangdong, China), Parrot Sequoia+ (Parrot, Paris, France), and MicaSense RedEdge MX (MicaSense, Seattle, WA, USA). The detailed information on their spectral bands is listed in Table 2. The hyperspectral wavelengths that were used for the synthetization of each band were located by looking for the closest one to the band head and the number of wavelengths needed to form the bandwidth. For example, eight hyperspectral bands from 441.33 to 456.81 nm were used to synthesize the blue band of P4 Multispectral. Additionally, to evaluate the performance in estimating potato N caused by hyperspectral bandwidths, three sets of broader bands were created by merging the reflectance values of 5, 9, and 18 hyperspectral wavelengths for mimicking the bandwidths of 10, 20, and 40 nm, respectively.

Table 2. True and synthesized spectral information of three widely used multispectral cameras.

Manufacturer	Model	Price	Spectral Bands	Band Center (nm)	Band Center (nm)	Synthesized Band Center (nm)	Synthesized Bandwidth (nm)
DJI	P4 Multispectral	\$6500 (Including a UAV)	Blue	450	16	449.07	15.48
			Green	560	16	559.65	15.48
			Red	650	16	650.32	15.48
			Red Edge	730	16	729.94	15.48
			NIR *	840	26	839.41	26.54
Parrot	Sequoia+	\$3500	Green	550	40	549.70	39.81
			Red	660	40	660.28	39.81
			Red Edge	735	10	736.57	11.06
			NIR *	790	40	790.76	39.81
Micasense	RedEdge MX	\$6300	Blue	475	32	475.61	33.17
			Green	560	27	560.75	26.54
			Red	668	14	666.91	13.27
			Red Edge	717	12	716.67	11.06
			NIR *	842	57	841.62	57.50

Note: The camera price represents an average value on the market; however, it varies among different vendors.
* NIR: near-Infrared.

As the spectral response varies by the wavelength of each multispectral band due to quantum properties of complementary metal-oxide semiconductor (CMOS) sensors [33,34], a spectral convolution process (Equation (1)) was applied to the hyperspectral reflectance for the synthesization. A spectral response function was used to create a set of weights for the hyperspectral wavelengths following a Gaussian distribution at a mean of the synthesized band center and standard deviation of half of the synthesized bandwidth to mimic the varied spectral responses [30,33,35].

$$R_i = \frac{\sum_j^n C_j R_j}{\sum_j^n C_j} \quad (1)$$

where R_i is the synthesized reflectance at each of the multispectral bands, R_j is the reflectance of the j th wavelength of the hyperspectral images with $j = 1, 2, \dots, 274$, and C_j are weights generated by the spectral response function. The collection of C_j for each synthesized multispectral band follows the Gaussian distribution with the mean of the central wavelength and the standard deviation equal to half of the bandwidth. n is the hyperspectral wavelength that is used to synthesize the multispectral band.

2.5. Data Analysis

All data analyses were performed in RStudio (Ver. 1.1.414, RStudio, Boston, MA, USA). The Pearson correlation was calculated between each image feature and ground data. To investigate the N variability of potato plants over the growing season, as well as the effects of N treatments on different potato varieties, the ground-measured leaf total N concentration and petiole nitrate-N concentration were fitted to the experimental factors using a linear mixed model using the 'lmer' function from the 'lme4' package [36] extended with the 'lmerTest' package [37], as shown in Equation (2).

$$y_{nijk} = \mu + D_n + F_i + V_k + \eta_{ik} + N_j + (F \times N \times V)_{ijk} + \varepsilon_{nijk} \quad (2)$$

where y_{nijk} is the leaf total N concentration or petiole nitrate-N concentration of the k th variety under the treatments of the i th fertigation and j th N rate, obtained during the n th data collection. μ is the grand mean. D_n is the main effect of the n th sampling date (representing the growth stages). F_i is the fixed effect of the i th fertigation type (i.e., fertigation or non-fertigation). V_k is the fixed effect of the k th variety (i.e., Colomba or Snowden). η_{ik} is the random whole-plot error. N_j is the fixed effect of the j th N rate. ε_{nijk} is the error term and follows $N(0, \sigma_\varepsilon^2)$, where σ_ε^2 is the common variance within all the treatments.

2.6. Model Development and Evaluation

A PLSR model was trained using the 'plsrf' function in the 'pls' package to estimate the total N concentration and petiole nitrate-N concentration by taking the image features as predictors. Testing the accuracy of the model performance was obtained in five-fold cross-validation (CV) of each fold randomly with 80% of the dataset as the training set and 20% as the testing set. In each fold, a PLSR model was fit with the validation method set as 'CV'. The testing estimates were predicted with an optimal number of components [38] that were returned by calling the 'selectNcomp' function [39,40] on the fitted model according to the standard error of its cross-validation residuals. The agreement between the true and estimates of the testing sets in the five folds was quantified as the R^2 and root mean square error (RMSE), normalized mean root square error (NRMSE), and Nash-Sutcliffe coefficient (NSE). Performances of the hyperspectral narrow bands (2.2 nm, the full spectra); broad bands (10, 20, and 40 nm); and three synthesized multispectral cameras were compared using these two metrics.

During the training process of PLSR models, information of the full set of predictors is projected into a smaller number of predictors so that variations in a reduced set of predictors (a principal component) are most likely to reflect the overall data variation [41].

The importance of a predictor is obtained by comparing its variation with the explained overall variations by all the principal components [42]. This importance can be returned as the Variable Importance in Projection (VIP) of the predictors in PLSR models using the 'VIP' function in the 'plsVarSel' package. Predictors with higher VIP scores contribute more toward the overall data variation. As the squared VIP scores average to 1, a predictor with a VIP score close to or greater than 1 can be considered important in a given model [41–43].

3. Results and Discussion

3.1. Potato N Variability by N Treatments

The variability of the potato N status over time is shown in Figure 2, and the treatment effects from the linear fit are listed in Table 3. The imaging dates had a significant and negative effect on the leaf total N, indicating that the total N level decreased as the potato plants reached maturity. The potato variety Snowden had higher total N concentrations in whole leaves generally under all treatments. The N application rate had a significantly positive effect, implying that, as more N was applied, the potato plants responded with a higher leaf total N, and both varieties responded at a similar rate. The interaction between imaging dates and the variety Snowden is also significant, which means that, during the growth of both varieties, the total N level of Snowden decreased faster than Colomba. It is noted that fertigation did not affect the level of the leaf total N concentration no matter how much N was applied.

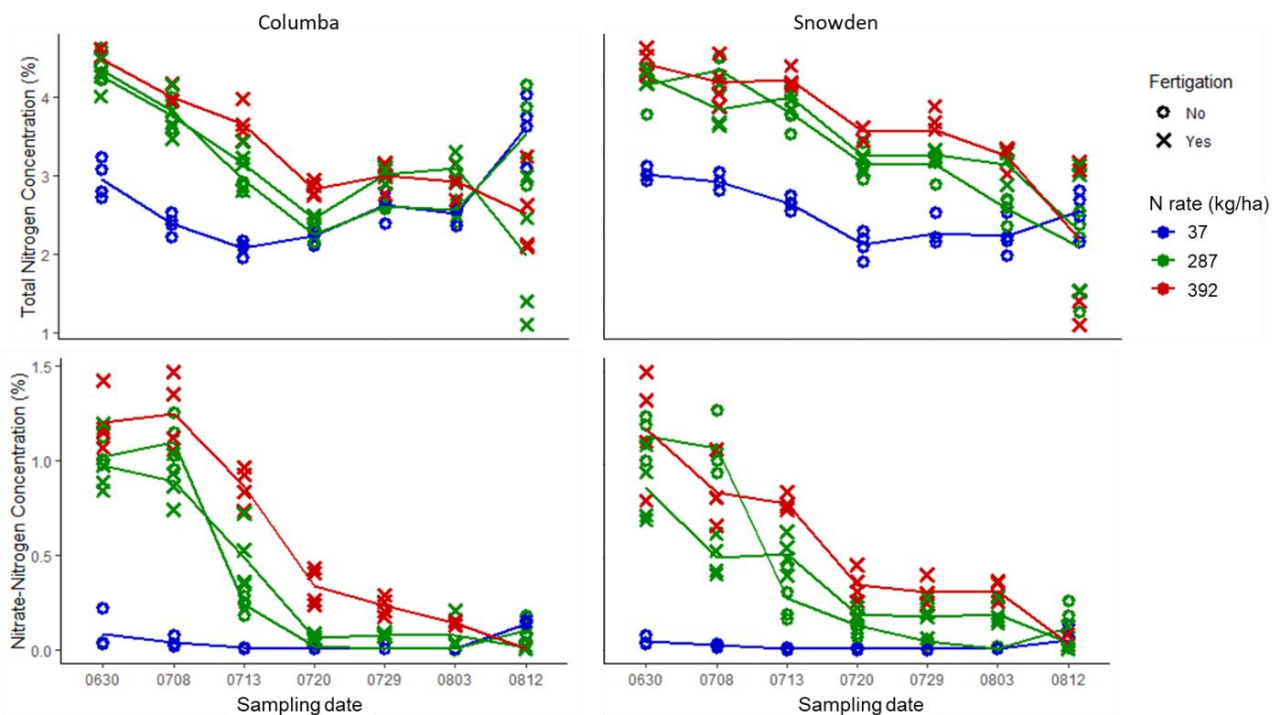


Figure 2. Potato leaf total N concentration and petiole nitrate-N concentration over the growing season for two varieties under different N treatments.

Similar to the total N concentration, significantly lower petiole nitrate-N concentrations were observed on the later dates of potato growth. Additionally, the more N applied to the plot, the higher petiole nitrate-N level the plants showed. Fertigation did not help potato plants gain more petiole nitrate-N in the petioles, no matter how much N was applied. Dissimilar to the leaf total N concentration, there was no difference in the petiole nitrate-N levels across varieties and N treatments. In summary, both N status indicators decreased as the potato plants got closer to maturity. The N application rate could significantly affect the N concentrations of potato plants, but fertigation could not.

Table 3. Effects of the experimental factors on potato N concentrations.

Coefficients	Leaf Total N Concentration (%)			Petiole Nitrate-N Concentration (%)		
	Sum of Sq [†]	F-Value	p-Value	Sum of Sq	F-Value	p-Value
Sampling Date	54.394	34.256	<0.001	19.326	65.192	<0.001
Fertigation	0.017	0.065	1.000	0.029	0.588	0.444
Variety	0.381	1.438	1.000	0.000	0.001	0.979
N rate	5.885	22.239	<0.001	2.800	56.671	<0.001
Fertigation: N rate	0.065	0.244	0.622	0.077	1.552	0.214
Fertigation: Variety	0.052	0.196	1.000	0.001	0.013	0.908
Variety: N rate	0.036	0.137	0.712	0.002	0.037	0.849
Variety: Fertigation: N rate	0.159	0.600	0.440	0.010	0.199	0.656

[†] Square.

3.2. Model Performance of the Hyperspectral Narrow and Broad Bands

The model performances from the five-fold CV of the PLSR model, taking each set of hyperspectral narrow and broad bands, are compared in Figure 3. The full spectra with 2.2 nm hyperspectral narrow bands reached the best testing accuracy with R^2 of 0.78 and RMSE of 0.41, which is around 12% of the average of the total N concentration (NRMSE), followed by the 10 nm bands, while for the petiole nitrate-N concentration, the 10 nm bands had the best performance ($R^2 = 0.87$, RMSE = 0.13, and NRMSE = 56.7%), followed by the full spectra. The model performance generally decreased as the bandwidth increased for both N status indicators.

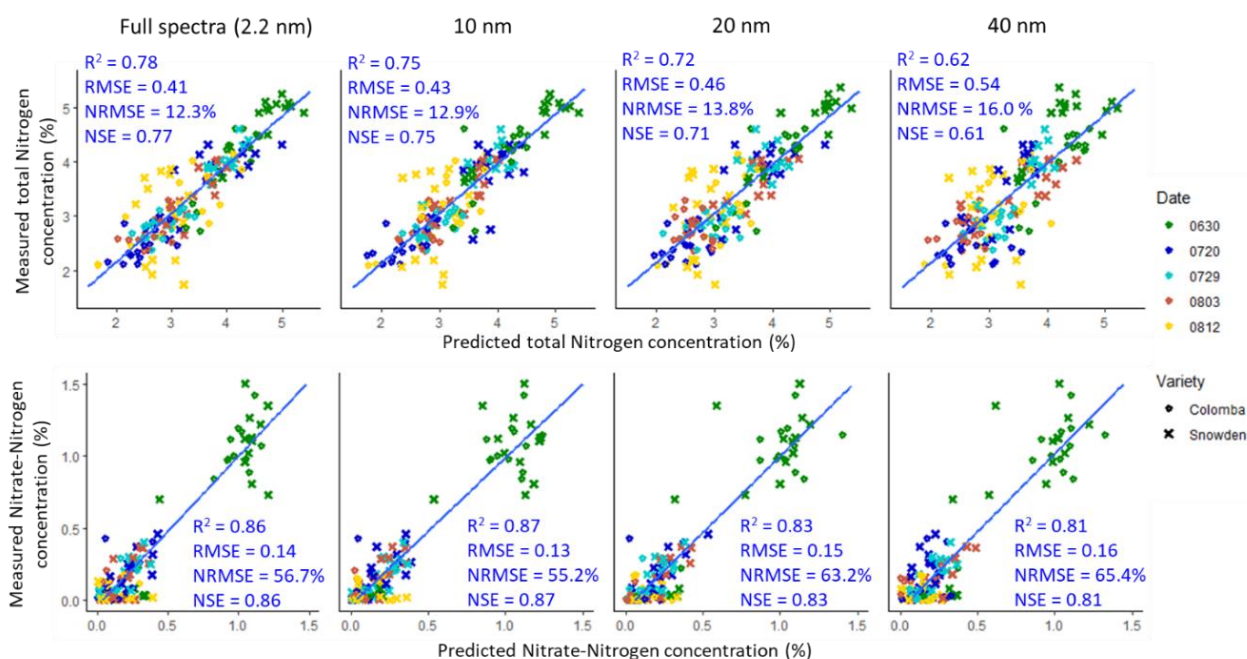


Figure 3. Scatterplots of the predicted and measured potato N concentrations. The predicted values were from PLSR models with the reflectance of hyperspectral narrow (2.2 nm) and broad bands (10, 20, and 40 nm). The blue solid line in each plot represents the line of $y = x$.

Our observations can be confirmed with previous studies that narrow bands in specific spectral regions dramatically improved the discrimination capabilities and estimation accuracies for crop vegetational traits, relative to broad bands [44,45]. Elvidge and Chen [46] showed that the narrow-band versions (4 nm) of VIs derived from ground spectrometer measurements had better linear correlations than their broad band counterparts (60–130 nm) in correlating with leaf area indices and green coverage of the pinyon pine canopy. Some other studies have shown that spectral resolutions in space-borne hyperspec-

tral data are more important than their spatial resolutions in forest characterization [47]. Comparing the effects in estimating the N levels by UAV spectral bands, through gradually aggregating the bandwidths from 10 to 40 nm, provides a reference to relative studies in selecting sensors and features to balance between the estimation performance and costs (in sensor, data management and storage, and computation).

3.3. Model Performance of the Hyperspectral and Synthesized Multispectral Reflectance

Figure 4 shows the comparisons of model performances among the hyperspectral reflectance and three synthesized multispectral cameras in estimating the potato N status. For both the leaf total N concentration and the petiole nitrate-N concentration, the hyperspectral full spectra largely outperformed all three multispectral cameras. There were no significant differences among the three brands of multispectral cameras.

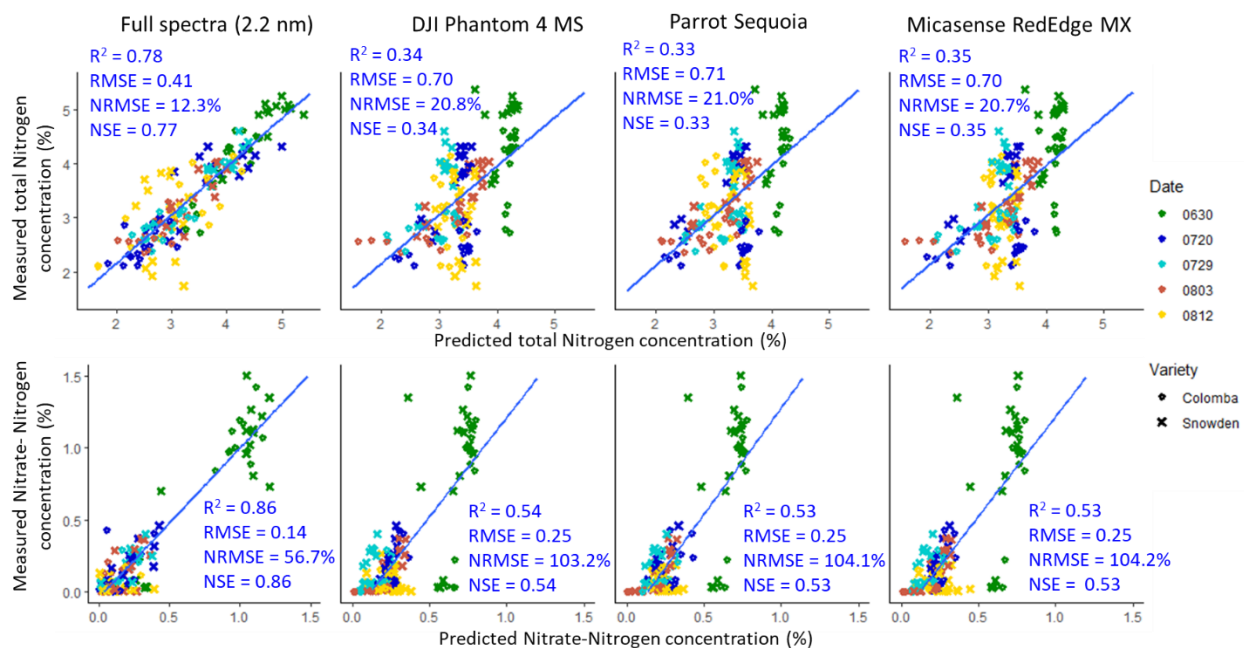


Figure 4. Scatterplots of the predicted and measured potato N concentrations. The predicted values were from PLSR models with the hyperspectral reflectance and synthesized reflectance of three popular multispectral cameras. The blue solid line in each plot represents the line of $y = x$.

The Pearson correlation coefficients (r) between reflectance values and the ground data are shown in Figure 5a,b. Reflectance in the visible range (<750 nm) had stronger correlations with either of the two N status indicators than the NIR region. The highest correlations ($|r| > 0.55$) for the total N concentration were located at the wavelengths around 430–470, 570–590, and 650–700 nm within the visible range, corresponding to the blue, green, and red bands of the multispectral cameras, respectively (see detailed bands and values in Supplementary Tables S1 and S2), while wavelengths around 550–600 and 700 nm are highly correlated ($|r| > 0.55$) with the petiole nitrate-N concentration, corresponding to the green and red bands. Similar conclusions were found in [15,48] that spectral bands in the visible regions were highly correlated with the potato canopy N status and in [16,17] that the red-edge regions were good linear estimators of potato N concentrations.

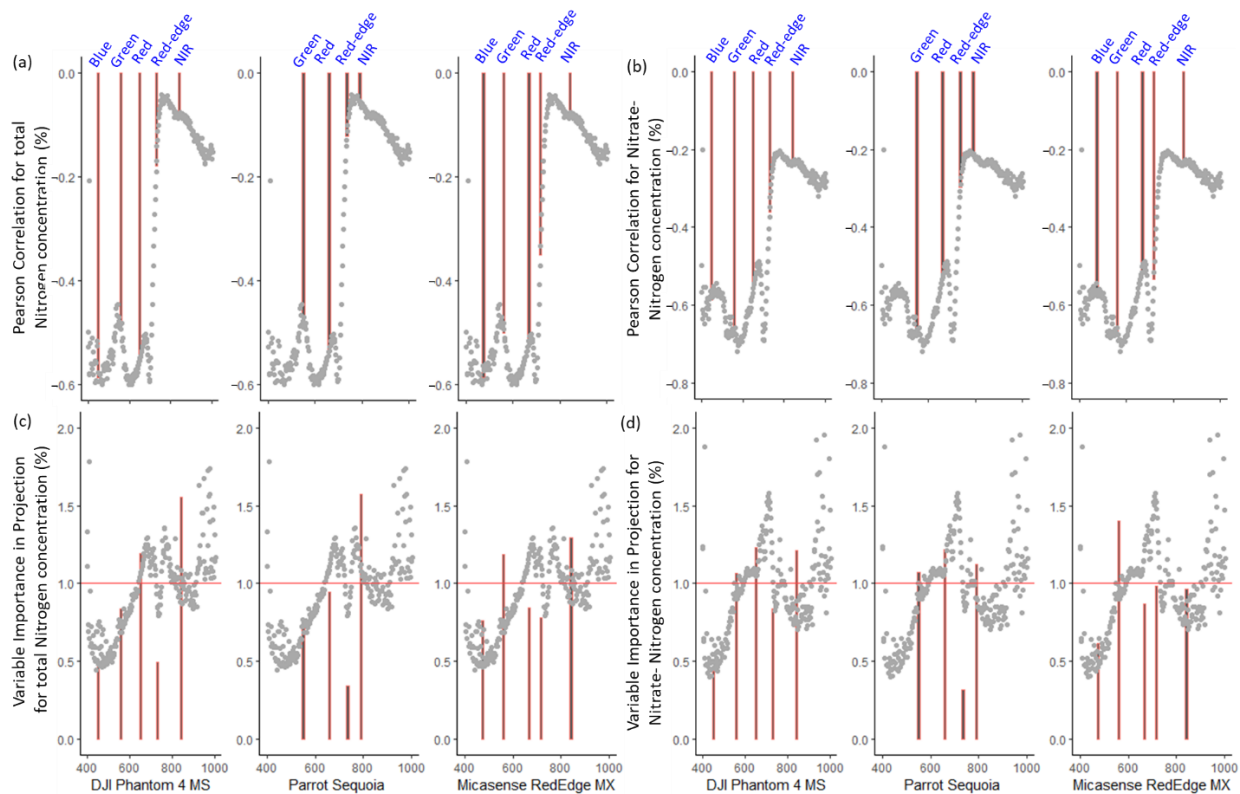


Figure 5. Bar plots of the variable importance of the imagery bands in estimating N concentrations. (a,b) Pearson correlations. (c,d) Variable Importance in Projections (VIPs). (a,c) The total N concentration, and (b,d) the petiole nitrate-N concentration. The gray dots represent hyperspectral wavelengths. The red horizontal line in (c,d) marks where the VIP score equals 1.

Though with broader bandwidths, the synthesized multispectral bands had similar correlations with the corresponding wavelengths in the hyperspectral spectra. No significant differences in the correlation coefficients were observed in the blue, green, red, and near-infrared bands among the three cameras. However, due to the steep changes of the correlations in the 700–750 nm region, the correlation coefficients in the red-edge band varied among cameras. The red-edge band of the MicaSense RedEdge MX (717 ± 12 nm) had the highest coefficients for both N concentrations, followed by the DJI P4 Multispectral (730 ± 16 nm). It was observed in this study that the closer a spectral band in the red-edge region is to the visible range, the higher correlations it had with the N concentrations.

The VIP scores in the PLSR model with different reflectance groups are shown in Figure 5c,d. It is worth noting that VIP scores measure the relative importance of predictors that were used to consist of the PLSR components. Wavelengths or bands with high values (>1) are considered significant based on the ‘greater than one rule’ but not necessarily indicating that the model would perform better than others. From the gray dots in Figure 5, the wavelengths between 650 and 830 nm and over 900 nm had VIP scores higher than 1. It can be clearly seen that the wavelength with high $|r|$ (430–470 and 570–590 nm) did not lead to high VIP scores, which might be caused by the high multicollinearity among the reflectance in the visible region (see detailed bands and values in Supplementary Tables S1 and S2). Instead, those over 900 nm had high importance to the model. Though with low correlations, they might serve in many of the PLSR components to explain the overall variation that was not reached by the high correlation ones.

In the synthesized multispectral reflectance, high VIPs scores in the visible regions only occurred in one of the bands, for example, the red band of the DJI P4 multispectral, while others were suppressed due to the multicollinearity. The low testing accuracy was also caused by the lack of compensation from spectral reflectance over 900 nm regions.

3.4. Effects of Potato Variety and Imaging Date on the Model Performance

The model performance for estimating the N concentrations for potato cultivars Colomba and Snowden was calculated separately and listed in Table 4. The best accuracy for the total N concentration within each of the cultivars was achieved by the 2.2 nm narrow bands, while the best one for the petiole nitrate-N concentration was the 10 nm bands, which, however, was very close to the performance of the full spectra. For both N concentrations estimated by the hyperspectral narrow bands, Colomba has slightly higher accuracies than Snowden. Moreover, Colomba showed consistently higher accuracies than Snowden in estimating the petiole nitrate-N concentrations using the hyperspectral broad bands or the synthesized multispectral reflectance, while Snowden had higher accuracies in estimating the total N concentration when using 20 nm and all the synthesized multispectral reflectance. Despite the slight difference, the overall accuracy ranges (R^2) were within 0.32–0.75 for Colomba and 0.37–0.72 for Snowden in estimating the leaf total N concentrations and were within 0.59–0.90 for Colomba and 0.46–0.84 for Snowden in estimating the petiole nitrate-N concentration. Therefore, we do not consider the two potato cultivars used in this study had a significant impact on the model performance.

Table 4. Model performance grouped by the two potato cultivars for the hyperspectral narrow and broad bands and the synthesized multispectral reflectance.

	Potato Cultivar	Full Spectra (2.2 nm)	10 nm	20 nm	40 nm	DJI Phantom 4 MS	Parrot Sequoia	Micasense RedEdge MX
Leaf total N concentration	Colomba	0.75 (0.39)	0.71 (0.41)	0.64 (0.46)	0.59 (0.52)	0.35 (0.69)	0.32 (0.71)	0.32 (0.72)
	Snowden	0.72 (0.44)	0.70 (0.46)	0.69 (0.47)	0.57 (0.56)	0.37 (0.71)	0.39 (0.70)	0.45 (0.68)
Petiole nitrate-N concentration	Colomba	0.90 (0.12)	0.90 (0.12)	0.86 (0.14)	0.86 (0.14)	0.59 (0.24)	0.59 (0.24)	0.60 (0.23)
	Snowden	0.83 (0.16)	0.84 (0.15)	0.80 (0.17)	0.78 (0.18)	0.49 (0.27)	0.49 (0.27)	0.46 (0.27)

Note: The numbers outside the parenthesis are the coefficients of determination (R^2), and the numbers within are the root mean square error (RMSE) between the model estimates and true values for each group. The best accuracy for each group among all seven image inputs was made bold.

The model performance for estimating the N concentrations using the input features collected on the five imaging dates was calculated separately and listed in Table 5. For the total N concentrations, the best accuracies were achieved by the 2.2 nm narrow bands on all the five imaging dates. When estimating the nitrate-N concentrations, the best accuracies on 06/30 and 08/03 were by the 10 nm broad bands, the best ones on 07/20 and 07/29 were by the 2.2 nm narrow bands, and the best one for 08/12 was by the 20 nm broad bands. None of the synthesized multispectral reflectance could outperform the hyperspectral bands.

Among the five imaging dates, the last date had significantly low accuracies for estimating both concentrations. It can be seen from Figure 2 that N concentrations gradually decreased over the growing season. The mean total N concentration values were 4.35 ± 0.72 , 3.08 ± 0.79 , 3.29 ± 0.64 , 3.13 ± 0.53 , and 2.94 ± 0.81 on the five imaging dates, respectively, and the mean nitrate-N concentration values were 0.82 ± 0.48 , 0.14 ± 0.14 , 0.11 ± 0.12 , 0.09 ± 0.12 , and 0.06 ± 0.07 on the five imaging dates, respectively. The N concentrations at the early dates were distributed averagely, and thus, the variations in the testing set could be fairly explained in the trained model. However, those on the last day occupied the leftmost sections of the distribution of all five days, making it difficult for the model to capture the subtle changes in the variations. Moreover, it was observed from Figures 3 and 4 that most outliers came from the last day. Thus, the imaging dates did have an impact on the model performance. The model currently trained with data collected throughout the season performed consistently well before potato plants entered the maturity stage (08/12).

Table 5. Model performance grouped by the five imaging dates for the hyperspectral narrow and broad bands and the synthesized multispectral reflectance.

	Imaging Date	Full Spectra (2.2 nm)	10 nm	20 nm	40 nm	DJI Phantom 4 MS	Parrot Sequoia+	Micasense RedEdge MX
Leaf total N concentration	06/30	0.83 (0.30)	0.76 (0.35)	0.77 (0.34)	0.39 (0.57)	0.01 (0.73)	0.02 (0.74)	0.01 (0.74)
	07/20	0.81 (0.36)	0.77 (0.40)	0.76 (0.39)	0.56 (0.52)	0.16 (0.73)	0.12 (0.78)	0.14 (0.77)
	07/29	0.89 (0.21)	0.81 (0.28)	0.64 (0.38)	0.74 (0.33)	0.20 (0.64)	0.27 (0.55)	0.22 (0.60)
	08/03	0.79 (0.25)	0.77 (0.25)	0.66 (0.37)	0.72 (0.38)	0.56 (0.39)	0.57 (0.35)	0.52 (0.41)
	08/12	0.25 (0.72)	0.22 (0.71)	0.19 (0.72)	0.13 (0.77)	0.01 (0.90)	0.07 (0.96)	0.00 (0.87)
Petiole nitrate-N concentration	06/30	0.81 (0.21)	0.82 (0.20)	0.76 (0.23)	0.76 (0.23)	0.20 (0.45)	0.25 (0.45)	0.16 (0.46)
	07/20	0.53 (0.11)	0.46 (0.11)	0.46 (0.12)	0.18 (0.14)	0.36 (0.19)	0.36 (0.23)	0.38 (0.19)
	07/29	0.70 (0.07)	0.66 (0.08)	0.53 (0.09)	0.55 (0.09)	0.37 (0.13)	0.40 (0.12)	0.38 (0.12)
	08/03	0.50 (0.09)	0.60 (0.08)	0.49 (0.10)	0.56 (0.12)	0.52 (0.13)	0.55 (0.11)	0.50 (0.14)
	08/12	0.04 (0.16)	0.04 (0.16)	0.20 (0.18)	0.18 (0.17)	0.06 (0.21)	0.00 (0.19)	0.06 (0.21)

Note: The numbers outside the parenthesis are the coefficients of determination (R^2), and the numbers within are the root mean square error (RMSE) between the model estimates and true values for each group. The best accuracy for each group among all seven image inputs is bold.

3.5. Model Performance for the Two N Concentrations

The regressing agreements for the petiole nitrate-N concentrations (Figures 3 and 4) might be overestimated due to its non-Gaussian distribution and cluster of outliers in the extended range. Moreover, when looking at the average error of the estimates given by the 2.2 nm narrow bands, the RMSE was over 56% of the mean petiole nitrate-N concentrations in the dataset, which is higher than the one for leaf N concentration (RMSE% = 12%). Potato plants absorb N from the soil mostly in the form of nitrate. Nitrate is transported to leaves through petioles, which connect each leaf to the main shoot. It was then reduced to ammonium and formed into organic N compounds [49]. The petiole nitrate-N concentration measures the proportion of nitrate reduction in the leaf in response to crop growth to the nitrate uptake by the potato root system. Therefore, it represents the short-term nutritional status of plants and can be used as an indicator of whether they are currently taking up enough nutrients [12]. The petiole nitrate-N concentration is generally preferred for giving nitrogenous fertilizer recommendations, as it is often reported to have significant correlations with the final tuber yield [11,12].

However, compared with the leaf N concentration, the petiole nitrate-N concentration could be more obscure to be measured through remote sensing equipment [21]. The sensitivity of spectral reflectance to the plant N concentration is explained by the correlations with the chlorophyll content and the fact that the amount of chlorophyll formed in plants is dependent on the amount of available N [50]. The spectral measurements of the plant canopy (leaf), thus, are expected to be correlated lower with the leaf spectral reflectance. Additionally, the activity of nitrate translocation highly depends on the transpiration rate of potato plants, which fluctuates due to changes in the solar radiation, air temperature, and stress. The precision of nitrate testing, even from potato petiole samples, is highly time- and environment-dependent [11].

On the other hand, the whole leaves indicating the cumulative nutritional status up to the present time can be better quantified by remote sensing measurements from plant canopies. The model performance for estimating the whole leaf N concentrations in this study reached a reasonable accuracy (R^2 of 0.78 and RMSE of 0.41) for practical use in monitoring the N status. However, the performance was less competitive compared to the previous studies by Cohen et al. [21] with an R^2 of 0.86 and Nigon et al. [22] with an R^2 of 0.79. The estimation accuracy is prone to be affected by a number of factors. The representation of plant N by leaf chlorophyll varies upon environmental conditions accumulated within the growing season, genotypic variations, and growth stages [51–53]. Furthermore, canopy spectral reflectance is, in fact, determined by leaf biophysical and biochemical properties, as well as plant canopy architecture [54]. Canopy reflectance

is considerably different than reflectance of individual leaves, as the canopy reflectivity could be altered by lower leaf layers, canopy positions, and background reflectance [55]. Therefore, estimating the leaf N concentration from canopy reflectance requires more robust sensing and modeling technologies to improve the accuracy.

3.6. Evaluation of the Sensor Costs and Performance

The costs to deliver the estimated potato N concentrations were evaluated in a broad way, including the costs of UAV platforms, sensors, and processing software. Similar to the hyperspectral imaging system used in this study, most off-the-shelf hyperspectral systems are integrated systems with a hyperspectral spectral camera, a GNSS-aided navigation system to ensure accurate georeferencing, radiometric calibration solutions, a processing tool, and/or some other sensors to ensure the data quality, which might lead to a total cost ranging from USD 10,000 to USD 100,000. The cost would be added on with the selection of a UAV platform varying between USD 3000 and USD 10,000. Multispectral cameras usually come with simpler packages with the camera itself, mounting kits to UAVs, and/or radiometric calibration panels. Multispectral camera manufacturers do not have specific tools for image processing. Therefore, the selection could be made from commercial software, such as Pix4Dmapper (Pix4D, Lausanne, Switzerland) and Agisoft MetaShape Professional (Agisoft LLC, St. Petersburg, Russia), to open-source software, OpenDroneMap (OpenDroneMap, 2020). Similarly, extra costs for purchasing a UAV platform are necessary for most multispectral cameras. One exception is made for the DJI P4 Multispectral, which comes with an integrated UAV imaging system. Prices of the three simulated multispectral cameras are listed in Table 2 for comparison. Additionally, with more spectral bands provided by the hyperspectral cameras (274 bands in this study), hyperspectral images take up significantly more data storage spaces on and off-board and, consequently, require higher computational capacities for processing, which needs to be counted into the total cost as well.

It can be seen from the previous analysis that the hyperspectral imagery outperformed the multispectral features, and there was no difference in the estimation accuracies among the three multispectral cameras. However, hyperspectral imaging systems cost more than multispectral systems. Although it is not an astonishing conclusion, the quantitative comparisons provide a reference for the trade-off between sensor costs and performance.

4. Conclusions

The performance of estimating potato N concentrations using narrow hyperspectral bands in the visible to NIR ranges and the broad multispectral bands was evaluated in the study. The leaf total N concentration and petiole nitrate-N concentration were obtained from 160 potato samples under four N treatments. Meanwhile, hyperspectral imagery was collected five times over the growing season, and a group of spectral reflectance values of multispectral bands was simulated. In this experiment, both N status indicators decreased as potato plants matured. The application of N could significantly improve the N concentrations of potato plants, but the fertigation practice could not. The best estimation accuracies were given by reflectance of the full spectra with 2.2 nm narrow with an R^2 of 0.78 and RMSE of 0.41 for the leaf total N concentration, while, for the petiole nitrate-N concentration, the 10 nm bands had the best performance ($R^2 = 0.87$ and RMSE = 0.13). The results also showed that spectral bands in the visible regions (400–700 nm) were the most highly correlated with the potato N levels among the visible–NIR range (400–1000 nm) that was investigated in this case. Thus, it can also be concluded from this study that performance in estimating potato N concentrations decreases as the increase of spectral bandwidth, and hyperspectral reflectance outperformed the simulated multispectral data for the three popular commercial cameras tested in this study. The systematic comparisons in this study serve as a reference for further studies in balancing the trade-off between sensor costs and performance.

Supplementary Materials: The following supporting information can be downloaded at: <https://www.mdpi.com/article/10.3390/agronomy12102533/s1>, Table S1: Pearson correlations and Variable Importance in Projection scores of the multispectral bands; Table S2: Pearson correlations and Variable Importance in Projection scores of the hyperspectral bands.

Author Contributions: B.W. and Y.M. collected the data. J.F. processed the data. J.Z. analyzed the data and wrote the first draft. Y.W. designed and supervised the experiment, reviewed, and edited the manuscript. Z.Z. conceptualized, reviewed, and edited the manuscript. All authors have read and agreed to the published version of the manuscript.

Funding: Funding was from the USDA National Institute of Food and Agriculture, Hatch project 1022709.

Data Availability Statement: The data and programming codes are freely available upon request.

Acknowledgments: We would like to thank Paul Sytsma and the field crew at the UW Hancock Agricultural Research Station for their kind help with field operations and management.

Conflicts of Interest: The authors declare that there are no conflicts of interest regarding the publication of this article.

References

1. Tilman, D.; Balzer, C.; Hill, J.; Befort, B.L. Global food demand and the sustainable intensification of agriculture. *Proc. Natl. Acad. Sci. USA* **2011**, *108*, 20260–20264. [[CrossRef](#)] [[PubMed](#)]
2. Prosekov, A.Y.; Ivanova, S.A. Food security: The challenge of the present. *Geoforum* **2018**, *91*, 73–77. [[CrossRef](#)]
3. Devaux, A.; Goffart, J.-P.; Kromann, P.; Andrade-Piedra, J.; Polar, V.; Hareau, G. The Potato of the Future: Opportunities and Challenges in Sustainable Agri-food Systems. *Potato Res.* **2021**, *64*, 681–720. [[CrossRef](#)] [[PubMed](#)]
4. Food and Agriculture Organization. International Year of the Potato 2008: New Light on a Hidden Treasure. Available online: <https://www.fao.org/potato-2008/en/events/book.html> (accessed on 11 February 2022).
5. U.S. Department of Agriculture. North American Potatoes. Available online: https://www.nass.usda.gov/Publications/Todays_Reports/reports/uscp0121.pdf (accessed on 11 February 2022).
6. Nigon, T.J.; Mulla, D.J.; Rosen, C.J.; Cohen, Y.; Alchanatis, V.; Rud, R. Evaluation of the nitrogen sufficiency index for use with high resolution, broadband aerial imagery in a commercial potato field. *Precis. Agric.* **2014**, *15*, 202–226. [[CrossRef](#)]
7. Weyermann, J.; Kneubühler, M.; Schläpfer, D.; Schaepman, M.E. Minimizing Reflectance Anisotropy Effects in Airborne Spectroscopy Data Using Ross–Li Model Inversion With Continuous Field Land Cover Stratification. *IEEE Trans. Geosci. Remote Sens.* **2015**, *53*, 5814–5823. [[CrossRef](#)]
8. Ward, M.H.; Jones, R.R.; Brender, J.D.; de Kok, T.M.; Weyer, P.J.; Nolan, B.T.; Villanueva, C.M.; van Breda, S.G. Drinking Water Nitrate and Human Health: An Updated Review. *Int. J. Environ. Res. Public Health* **2018**, *15*, 1557. [[CrossRef](#)]
9. Rosen, C.J.; Bierman, P.M. Best Management Practices for Nitrogen Use: Irrigated Potatoes. Available online: <https://conservancy.umn.edu/bitstream/handle/11299/198232/n-bmps-irrigated-potatoes-2008.pdf?sequence=1> (accessed on 11 February 2022).
10. Liu, N.; Townsend, P.A.; Naber, M.R.; Bethke, P.C.; Hills, W.B.; Wang, Y. Hyperspectral imagery to monitor crop nutrient status within and across growing seasons. *Remote Sens. Environ.* **2021**, *255*, 112303. [[CrossRef](#)]
11. Zhang, H.; Smeal, D.; Arnold, R.; Gregory, E. Potato nitrogen management by monitoring petiole nitrate level. *J. Plant Nutr.* **1996**, *19*, 1405–1412. [[CrossRef](#)]
12. Wang, Y.; Naber, M.; Crosby, T.; Liang, G. Evaluating Multiple Diagnostic Tools for Monitoring In-season Nitrogen Status of Chipping Potatoes in the Upper Midwest of the USA. *Potato Res.* **2021**, *65*, 31–50. [[CrossRef](#)]
13. Bélanger, G.; Walsh, J.; Richards, J.; Milburn, P.; Ziadi, N. Critical petiole nitrate concentration of two processing potato cultivars in eastern Canada. *Am. J. Potato Res.* **2003**, *80*, 251–261. [[CrossRef](#)]
14. Kaiser, D.E.; Rosen, C.J. Understanding Plant Analysis for Crops. Available online: <https://extension.umn.edu/testing-and-analysis/understanding-plant-analysis-crops> (accessed on 11 February 2022).
15. Yang, H.; Li, F.; Hu, Y.; Yu, K. Hyperspectral indices optimization algorithms for estimating canopy nitrogen concentration in potato (*Solanum tuberosum* L.). *Int. J. Appl. Earth Obs. Geoinf.* **2021**, *102*, 102416. [[CrossRef](#)]
16. Clevers, J.G.P.W.; Kooistra, L. Using Hyperspectral Remote Sensing Data for Retrieving Canopy Chlorophyll and Nitrogen Content. *IEEE J. Sel. Top. Appl. Earth Obs. Remote Sens.* **2012**, *5*, 574–583. [[CrossRef](#)]
17. Morier, T.; Cambouris, A.N.; Chokmani, K. In-Season Nitrogen Status Assessment and Yield Estimation Using Hyperspectral Vegetation Indices in a Potato Crop. *Agron. J.* **2015**, *107*, 1295–1309. [[CrossRef](#)]
18. Herrmann, I.; Karnieli, A.; Bonfil, D.J.; Cohen, Y.; Alchanatis, V. SWIR-based spectral indices for assessing nitrogen content in potato fields. *Int. J. Remote Sens.* **2010**, *31*, 5127–5143. [[CrossRef](#)]
19. Sun, H.; Li, M.; Zhang, Q.; Alva, A.K.; Zhou, Z. Preliminary study on nitrogen monitoring of potato plants using multispectral image. In Proceedings of the American Society of Agricultural and Biological Engineers Annual International Meeting 2013, ASABE, Kansas City, MO, USA, 21–24 July 2013; pp. 4007–4013.

20. Zhou, Z.; Jabloun, M.; Plauborg, F.; Andersen, M.N. Using ground-based spectral reflectance sensors and photography to estimate shoot N concentration and dry matter of potato. *Comput. Electron. Agric.* **2018**, *144*, 154–163. [CrossRef]
21. Cohen, Y.; Rud, R.; Rosen, C.; Mulla, D.; Heuer, B.; Dar, Z.; Levi, O.; Cohen, S.; Levi, A.; Brikman, R.; et al. The use of VIS-NIR and thermal ranges for evaluating nitrogen and water status in potato plants. In Proceedings of the Precision Agriculture 2011-Papers Presented at the 8th European Conference on Precision Agriculture 2011, Prague, Czech Republic, 11–14 July 2011; pp. 99–108.
22. Nigon, T.J.; Mulla, D.J.; Rosen, C.J.; Cohen, Y.; Alchanatis, V.; Knight, J.; Rud, R. Hyperspectral aerial imagery for detecting nitrogen stress in two potato cultivars. *Comput. Electron. Agric.* **2015**, *112*, 36–46. [CrossRef]
23. Hunt, E.R.; Horneck, D.A.; Spinelli, C.B.; Turner, R.W.; Bruce, A.E.; Gadler, D.J.; Brungardt, J.J.; Hamm, P.B. Monitoring nitrogen status of potatoes using small unmanned aerial vehicles. *Precis. Agric.* **2018**, *19*, 314–333. [CrossRef]
24. Yang, C.; Everitt, J.H. Comparison of hyperspectral imagery with aerial photography and multispectral imagery for mapping broom snakeweed. *Int. J. Remote Sens.* **2010**, *31*, 5423–5438. [CrossRef]
25. Sun, J.; Yang, J.; Shi, S.; Chen, B.; Du, L.; Gong, W.; Song, S. Estimating Rice Leaf Nitrogen Concentration: Influence of Regression Algorithms Based on Passive and Active Leaf Reflectance. *Remote Sens.* **2017**, *9*, 951. [CrossRef]
26. Lee, K.-S.; Cohen, W.B.; Kennedy, R.E.; Maiersperger, T.K.; Gower, S.T. Hyperspectral versus multispectral data for estimating leaf area index in four different biomes. *Remote Sens. Environ.* **2004**, *91*, 508–520. [CrossRef]
27. Sluiter, R.; Pebesma, E.J. Comparing techniques for vegetation classification using multi-and hyperspectral images and ancillary environmental data. *Int. J. Remote Sens.* **2010**, *31*, 6143–6161. [CrossRef]
28. Marshall, M.; Thenkabail, P. Advantage of hyperspectral EO-1 Hyperion over multispectral IKONOS, GeoEye-1, WorldView-2, Landsat ETM+, and MODIS vegetation indices in crop biomass estimation. *ISPRS J. Photogramm. Remote Sens.* **2015**, *108*, 205–218. [CrossRef]
29. Tong, A.; He, Y. Estimating and mapping chlorophyll content for a heterogeneous grassland: Comparing prediction power of a suite of vegetation indices across scales between years. *ISPRS J. Photogramm. Remote Sens.* **2017**, *126*, 146–167. [CrossRef]
30. Lu, B.; He, Y.; Dao, P.D. Comparing the Performance of Multispectral and Hyperspectral Images for Estimating Vegetation Properties. *IEEE J. Sel. Top. Appl. Earth Obs. Remote Sens.* **2019**, *12*, 1784–1797. [CrossRef]
31. Kniffin, M. Sustaining Central Sands Water Resources. Ph.D. Thesis, University of Wisconsin-Madison, Madison, WI, USA, 2014.
32. University of Wisconsin Soil and Forage Lab. Lab Procedures and Methods. Available online: https://uwlab.webhosting.cals.wisc.edu/wp-content/uploads/sites/17/2015/10/potato_N.pdf (accessed on 11 February 2022).
33. Lu, B.; He, Y. Species classification using Unmanned Aerial Vehicle (UAV)-acquired high spatial resolution imagery in a heterogeneous grassland. *ISPRS J. Photogramm. Remote Sens.* **2017**, *128*, 73–85. [CrossRef]
34. Del Pozo, S.; Rodríguez-González, P.; Hernández-López, D.; Felipe-García, B. Vicarious Radiometric Calibration of a Multispectral Camera on Board an Unmanned Aerial System. *Remote Sens.* **2014**, *6*, 1918–1937. [CrossRef]
35. Von Bueren, S.K.; Burkart, A.; Hueni, A.; Rascher, U.; Tuohy, M.P.; Yule, I.J. Deploying four optical UAV-based sensors over grassland: Challenges and limitations. *Biogeosciences* **2015**, *12*, 163–175. [CrossRef]
36. Bates, D.; Mächler, M.; Bolker, B.; Walker, S. Fitting Linear Mixed-Effects Models Using lme4. *J. Stat. Softw.* **2015**, *67*, 1–48. [CrossRef]
37. Kuznetsova, A.; Brockhoff, P.B.; Christensen, R.H.B. lmerTest Package: Tests in Linear Mixed Effects Models. *J. Stat. Softw.* **2017**, *82*, 1–26. [CrossRef]
38. Wiklund, S.; Nilsson, D.; Eriksson, L.; Sjöström, M.; Wold, S.; Faber, K. A randomization test for PLS component selection. *J. Chemom. A J. Chemom. Soc.* **2007**, *21*, 427–439. [CrossRef]
39. Mevik, B.-H.; Wehrens, R. Introduction to the pls Package. Available online: <https://cran.r-project.org/web/packages/pls/vignettes/pls-manual.pdf> (accessed on 11 February 2022).
40. Hastie, T.; Tibshirani, R.; Friedman, J.H.; Friedman, J.H. *The Elements of Statistical Learning: Data Mining, Inference, and Prediction*; Springer: Berlin/Heidelberg, Germany, 2009; Volume 2.
41. Mukherjee, R.; Sengupta, D.; Sikdar, S.K. Selection of Sustainable Processes Using Sustainability Footprint Method: A Case Study of Methanol Production from Carbon Dioxide. In *Computer Aided Chemical Engineering*; You, F., Ed.; Elsevier: Amsterdam, The Netherlands, 2015; Volume 36, pp. 311–329.
42. Wang, Z.X.; He, Q.P.; Wang, J. Comparison of variable selection methods for PLS-based soft sensor modeling. *J. Process Control.* **2015**, *26*, 56–72. [CrossRef]
43. Zhou, J.; Yungbluth, D.; Vong, C.N.; Scaboo, A.; Zhou, J. Estimation of the maturity date of soybean breeding lines using UAV-based multispectral imagery. *Remote Sens.* **2019**, *11*, 2075. [CrossRef]
44. Thenkabail, P.S.; Enclona, E.A.; Ashton, M.S.; Van Der Meer, B. Accuracy assessments of hyperspectral waveband performance for vegetation analysis applications. *Remote Sens. Environ.* **2004**, *91*, 354–376. [CrossRef]
45. Santos-Rufo, A.; Mesas-Carrascosa, F.-J.; García-Ferrer, A.; Meroño-Larriva, J.E. Wavelength Selection Method Based on Partial Least Square from Hyperspectral Unmanned Aerial Vehicle Orthomosaic of Irrigated Olive Orchards. *Remote Sens.* **2020**, *12*, 3426. [CrossRef]
46. Elvidge, C.D.; Chen, Z. Comparison of broad-band and narrow-band red and near-infrared vegetation indices. *Remote Sens. Environ.* **1995**, *54*, 38–48. [CrossRef]

47. Thenkabail, P.S.; Hall, J.; Lin, T.; Ashton, M.S.; Harris, D.; Enclona, E.A. Detecting floristic structure and pattern across topographic and moisture gradients in a mixed species Central African forest using IKONOS and Landsat-7 ETM+ images. *Int. J. Appl. Earth Obs. Geoinf.* **2003**, *4*, 255–270. [[CrossRef](#)]
48. Herrmann, I.; Bdolach, E.; Montekyo, Y.; Rachmilevitch, S.; Townsend, P.A.; Karnieli, A. Assessment of maize yield and phenology by drone-mounted superspectral camera [Article]. *Precis. Agric.* **2019**, *21*, 51–76. [[CrossRef](#)]
49. Bernie Zebarth, G.M.; Charles, K. Nitrogen Management for Potatoes: Petiole Nitrate Testing. Available online: https://www2.gnb.ca/content/dam/gnb/Departments/10/pdf/Agriculture/potato_pnit.pdf (accessed on 11 February 2022).
50. Stroppiana, D.; Fava, F.; Boschetti, M.; Brivio, P. Estimation of nitrogen content in crops and pastures using hyperspectral vegetation indices. In *Hyperspectral Remote Sensing of Vegetation*; Thenkabail, P.S., Lyon, J.G., Huete, A., Eds.; CRC Press: Boca Raton, FL, USA, 2011; pp. 245–262.
51. Filella, I.; Serrano, L.; Serra, J.; Penuelas, J. Evaluating wheat nitrogen status with canopy reflectance indices and discriminant analysis. *Crop Sci.* **1995**, *35*, 1400–1405. [[CrossRef](#)]
52. Houles, V.; Guerif, M.; Mary, B. Elaboration of a nitrogen nutrition indicator for winter wheat based on leaf area index and chlorophyll content for making nitrogen recommendations. *Eur. J. Agron.* **2007**, *27*, 1–11. [[CrossRef](#)]
53. Hatfield, J.L.; Gitelson, A.A.; Schepers, J.S.; Walthall, C.L. Application of spectral remote sensing for agronomic decisions. *Agron. J.* **2008**, *100*, S-117–S-131. [[CrossRef](#)]
54. Daughtry, C.S.T.; Walthall, C.L.; Kim, M.S.; de Colstoun, E.B.; McMurtrey, J.E. Estimating Corn Leaf Chlorophyll Concentration from Leaf and Canopy Reflectance. *Remote Sens. Environ.* **2000**, *74*, 229–239. [[CrossRef](#)]
55. Knipling, E.B. Physical and physiological basis for the reflectance of visible and near-infrared radiation from vegetation. *Remote Sens. Environ.* **1970**, *1*, 155–159. [[CrossRef](#)]